pubs.acs.org/acschemicalbiology

Articles

Optochemical Control of TET Dioxygenases Enables Kinetic Insights into the Domain-Dependent Interplay of TET1 and MBD1 while Oxidizing and Reading 5-Methylcytosine

Published as part of the ACS Chemical Biology special issue "Epigenetics 2022".

Tzu-Chen Lin, Shubhendu Palei, and Daniel Summerer*

Cite This: *ACS Chem. Biol.* 2022, 17, 1844−1852

Read Online

ACCESS | Metrics & More | Article Recommendations | Supporting Information

ABSTRACT: Methyl-CpG binding domain (MBD) proteins and ten-eleven-translocation (TET) dioxygenases are the readers and erasers of 5-methylcytosine (5mC), the central epigenetic mark of mammalian DNA. We employ light-activatable human TET1 controlled by a genetically encoded photocaged serine to enable in vivo kinetic studies of their interplay at the common substrate methylated cytosine−guanine (mCpG). We identify the multidomain reader MBD1 to negatively regulate TET1-catalyzed 5mC oxidation kinetics via its mCpG-binding MBD domain. However, we also identify the third Cys-x-x-Cys (CXXC3) domain of MBD1 to promote oxidation kinetics by TET1, dependent on its ability to bind nonmethylated CpG, the final product of TET-mediated mCpG oxidation and active demethylation. In contrast, we do not observe differences in TET1 regulation for MBD1 variants with or without the transcriptional repressor domain. Our approach reveals a complex, domain-dependent interplay of these readers and erasers of 5mC with different domain-specific contributions of MBD1 to the overall kinetics of TET1-catalyzed global 5mC oxidation kinetics that contribute to a better understanding of dynamic methylome shaping.

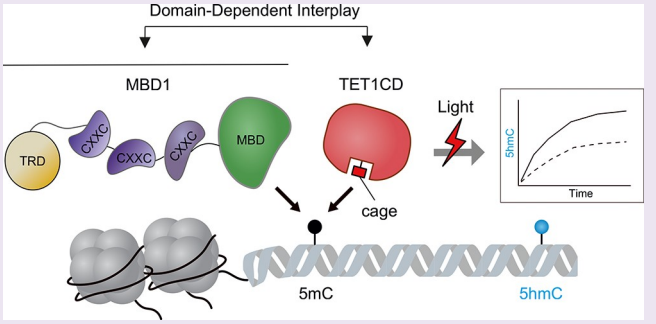

1. INTRODUCTION

5-Methylcytosine (5mC, Figure 1) is a dynamic regulatory element of mammalian genomes with important roles in transcription regulation, differentiation, and development.[1] 5mC is written and erased predominantly at cytosine−guanine (CpG) dinucleotides by DNA methyl transferases (DNMT) and ten-eleven-translocation (TET) dioxygenases, respectively.[2] Methyl-CpG binding domain (MBD)-containing proteins are the main readers of methylated CpG (mCpG) and interpret the methylome by coordinating crosstalk between 5mC, histone modifications, and other regulatory elements, typically leading to chromatin condensation and transcriptional silencing.[3] The MBD core family proteins (comprising MBD1, MBD2, MBD3, MBD4, and MeCP2, Figure 2a) are characterized by a conserved 70−85 aa MBD domain capable of recognizing methylated CpGs (mCpGs; except MBD3 that contains a dysfunctional MBD). In contrast, the individual MBD proteins substantially differ in additional interactor domains that equip them with distinct functions in chromatin regulation.[3]

Active reversal of 5mC is a crucial part of dynamic epigenetic regulation and, in mammals, is initiated by the

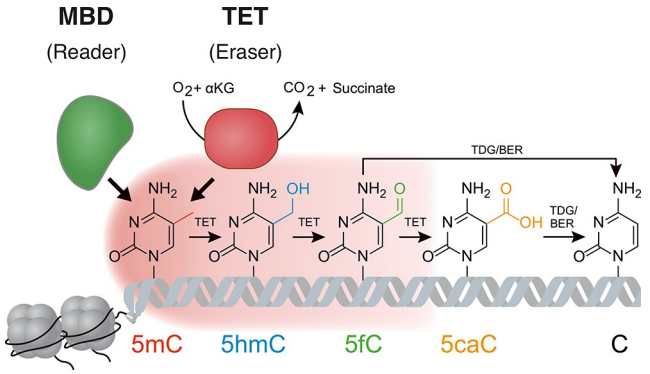

Figure 1. Cartoon illustrating the interplay between TETs and MBDs at their common 5mC substrate as the key process of epigenome regulation. MBD proteins read 5mC and translate it into regulatory signals, while TETs oxidize 5mC and mediate active demethylation.

Received: March 21, 2022
Accepted: May 18, 2022
Published: June 16, 2022

https://doi.org/10.1021/acschembio.2c00245
ACS Chem. Biol. 2022, 17, 1844−1852

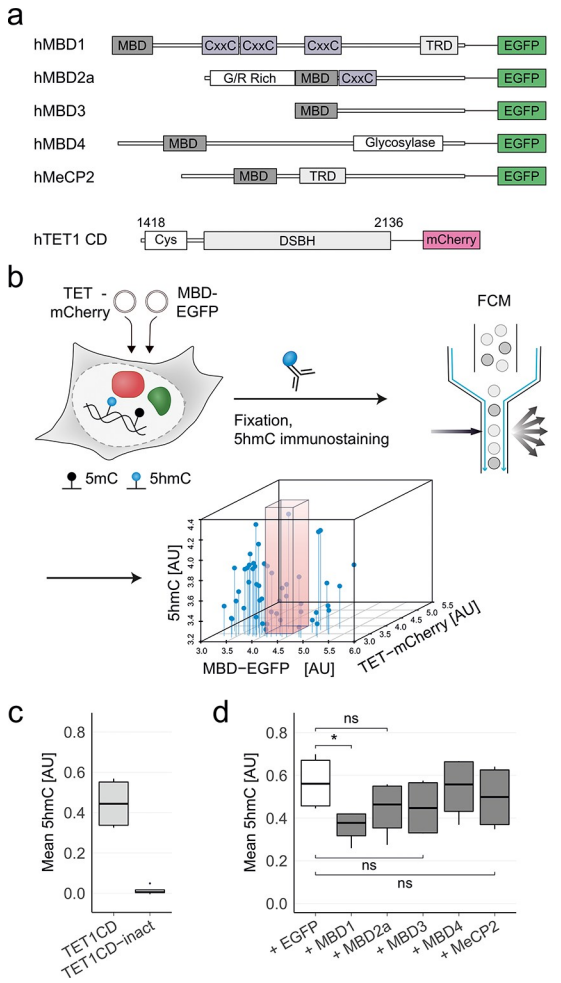

Figure 2. Modulation of TET1-catalyzed 5mC oxidation by human MBD proteins. (a) Domain structures of the five human core family MBD proteins (CXXC, Cys-x-x-Cys domain; TRD, transcriptional repressor domain) and the catalytic domain of human TET1 (Cys: cysteine-rich domain; DSBH: double-stranded β-helix domain). (b) FCM workflow and selected cell group for further analyses. (c) FCM analysis of cells expressing active or inactive TET1CD-mCherry immunostained for 5hmC. Measurements were conducted 16 h after transfection. Median intensity of 5hmC immunofluorescence from >100 cells was normalized to the median 5hmC immunofluorescence intensity of the untransfected cell population (Figure S1). Data are from four independent biological replicates. (d) FCM analysis of cells as in Figure 2c under coexpression of different MBD-EGFP constructs. p values from an unpaired student's t test of four independent biological replicates (*: $p \leq 0.05$; ns: $p > 0.05$).

ten-eleven-translocation (TET) dioxygenases TET1, TET2, and TET3. TETs iteratively oxidize 5mC to 5-hydroxymethylcytosine, 5-formylcytosine, and 5-carboxylcytosine (5hmC, 5fC, and 5caC, Figure 1) in an oxygen-, Fe(II)-, and α-ketoglutarate (α-KG)-dependent manner.[2,4] These oxidized 5mC derivatives are intermediates of active demethylation that occurs via the base excision repair pathway but have additionally been shown to uniquely interact with DNA-binding proteins to alter gene expression.[5−9]

The interplay of MBD proteins and TETs at their common mCpG target is dynamic and highly regulated in the mammalian genome to achieve a regular transcription program.[10] The study of this interplay can thus provide a mechanistic understanding of disease-causing, aberrant methylation-associated events. For example, a recent study has shown that MBD2 and MeCP2 confine the access of TET1 to its 5mC substrate and thereby prevent aberrant TET activity in a mouse model for Rett syndrome.[11]

It has also been shown that murine MBD1 and TET1 interact, leading to an MBD1-CXXC3-dependent TET1 (where CXXC3 is the third Cys-x-x-Cys) recruitment to mouse pericentromeric heterochromatin and enhanced 5hmC formation.[12] The study of the regulation of TETs by MBDs directly on the level of TET-mediated 5mC oxidation kinetics in chromatin would be highly valuable to better understand these processes but depends on the ability to directly control TET catalysis in cells with high temporal resolution. This would enable the uncoupling of the oxidation kinetics from the kinetics of upstream processes in the TET/MBD life cycles and thus provide a more unperturbed picture of their interplay.

Here, we employ light-activatable TET dioxygenases[13] to study the intracellular regulation of TET1-mediated global 5mC oxidation by MBDs in a human model system. Genetic encoding of a photocaged serine in the TET1 active site enables its translation in an inactive state, followed by its light activation and monitoring of global 5hmC formation in a virtually 5hmC-free genomic background. Coexpression of TET1 with the five human core family MBDs leads to differential modulation of oxidation with MBD1 acting as a negative regulator. Subsequent kinetic studies with photocaged TET1 and MBD1 variants lacking the MBD, CXXC3, or TRD domain or bearing dysfunctional domain mutants hint at a complex interplay between MBD1 and TET1 that involves a downregulation of 5mC oxidation that depends on the ability of the MBD domain to bind mCpG but also an activation that depends on the ability of the MBD1 CXXC3 domain to bind nonmethylated CpGs. In contrast, we do not observe regulation by the transcriptional repressor domain (TRD), suggesting that a potential indirect regulation of TET1 by a TRD-mediated chromatin condensation is not initially relevant in our model system.

2. RESULTS AND DISCUSSION

2.1. A Coexpression Screen of Human MBD Proteins and TET1 Reveals a Downregulation of TET1 Activity by MBD1.

Previous studies have shown the ability of several core family MBDs to alter TET functions in different organisms and genomic contexts.[10−12,14−16] For our study, we aimed to first get a comparative overview of how the presence of human core family MBDs would modulate the activity of human TET1 on the global level in the cell model system we planned to apply. We conducted a functional screen of TET1 activity by transiently coexpressing enhanced green fluorescent protein (EGFP)-tagged human full-length MBD proteins (MBD1, MBD2, MBD3, MBD4, and MeCP2, Figure 2a) and mCherry-tagged human TET1CD (catalytic domain, Figure 2a)[17] in HEK293T cells (the same tagging strategy was used for later experiments and is indicated in the figures, but for simplicity, we do not include the tag in the protein names). We thereby chose to focus on the catalytic domain of hTET1, since it behaved similar to the full-length hTET1 in an imaging-based chromocenter study by Cardoso and co-workers.[12] Moreover, expression of the catalytic domain provides higher 5hmC signals. We fixed the cells 16 h after transfection and measured global 5hmC formation on the single cell level by immunofluorescence labeling of 5hmC and FCM (flow cytometry)-assisted detection (Figure 2b). We initially

https://doi.org/10.1021/acschembio.2c00245
ACS Chem. Biol. 2022, 17, 1844−1852

grouped the FCM data by EGFP and mCherry intensities to individually measure the differential modulation of TET1 activity at different MBD/TET expression ratios. To screen within a useful dynamic range in subsequent experiments, we defined a specific group with a medium TET expression level and high MBD expression levels (Figure 2b; this ratio provides a high 5hmC signal over the background, Figure 2c).

We observed a trend for slightly decreased TET1-catalyzed 5hmC formation for MeCP2 and MBD2 as compared to the EGFP-only negative control, which is in agreement with a previous study conducted in HEK293T and mouse myoblasts cells (Figure 2d).[11] Coexpression of MBD3 also led to a trend for slight reduction, whereas MBD4 did not affect 5hmC formation. In contrast, coexpression of MBD1 led to a strong and significant reduction of the 5hmC formation (Figure 2d). Interestingly, the opposite was previously observed for mouse TET1CD and MBD1 without light control. Imaging studies in mouse fibroblasts showed a colocalization of both proteins at pericentromeric heterochromatin, alongside a promotion of the TET1-mediated 5hmC formation.[12] This discrepancy may be due to differences between the human and murine proteins or employed cell types. Moreover, whereas FCM analysis provides data on global 5hmC, the employed imaging experiments specifically reveal the 5hmC formation in mouse-specific pericentromer DNA.

2.2. Kinetic Studies with Light-Activatable TET1 Hint at a Competition between MBD1 and TET1 at mCpG. Given the significant downregulation of TET1-catalyzed 5mC oxidation by MBD1, we focused on this MBD for subsequent kinetic studies. We have recently reported the direct light activation of TET dioxygenases in cells by the incorporation of 4,5-dimethoxy-2-nitrobenzyl-L-serine (**1**, Figure 3a) via amber suppression.[18] We replaced the active site serine S2045 with this photocaged derivative in order to position the 4,5-dimethoxy-2-nitrobenzyl-group for steric clash with the bound α-KG and Fe(II)[13] and, therefore, to enable caging of the catalytic activity.[19−21] In this way, it becomes possible to translate TET1 in a catalytically inactive state and activate it at desired time points with high spatiotemporal resolution. This allows one to uncouple the kinetics of TET1 catalysis from the kinetics of upstream processes for precise measurements of its modulation by MBD1.

To adapt this approach for our study, we constructed a vector encoding hTET1CD with a single in-frame amber codon at S2045 and a C-terminal mCherry domain to faithfully monitor the expression of the caged TET1 catalytic domain by fluorescence (Figure 3b). In HEK293T cells cotransfected with a vector encoding an evolved *Escherichia coli* amber suppressor leucyl-tRNA-synthetase (LRS)/$tRNA^{Leu}$ pair, we observed a significantly higher mCherry expression in the presence of 0.05 mM **1** as compared to its absence, indicating a high fidelity of incorporation (Figures 3c and S2). We next validated whether hTET1CD-S2045 → **1** was successfully translated in an inactive state and if it could be activated with light in vivo. We added 0.05 mM **1** 3 h after transfection, grew the cells for 21 h, replaced the medium with prewarmed PBS to stop the expression of hTET1CD-S2045 → **1**, and irradiated the cells with light (365 nm, 15 W) for 3 min. The cells showed a rapid 5hmC increase with an initial linear behavior in a 4 h time window after irradiation, whereas nonirradiated cells showed low 5hmC signals even after 4 h (Figure 3d, upper panel, black and white triangles). mCherry signals indicated a stable TET1 expression level over the whole 4 h, showing that the 5hmC

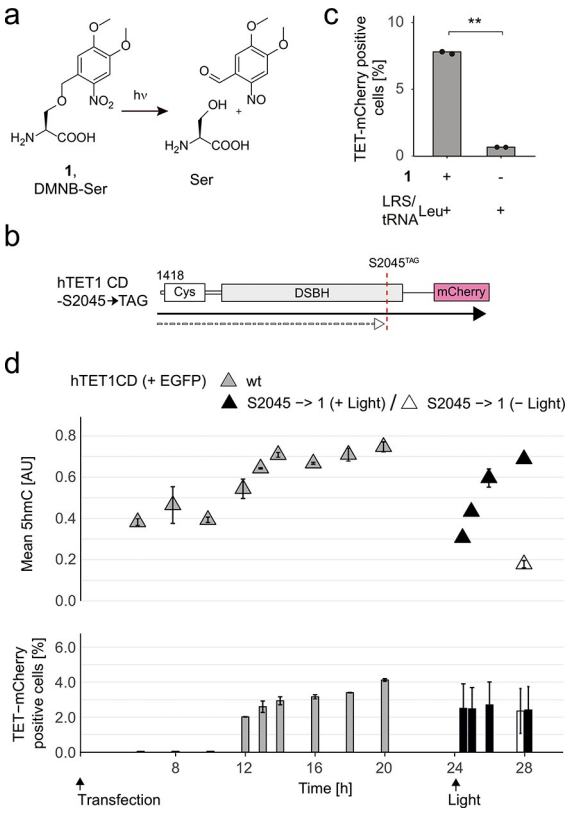

Figure 3. Light activation of TET1 for kinetic studies of 5hmC formation in HEK293T cells. (a) Reaction scheme for the decaging of **1**. (b) Domain structure of hTET1CD-S2045 → TAG with C-terminal mCherry. (c) Incorporation fidelity for **1** at hTET1CD S2045 → TAG codon assessed by FCM analysis of the mCherry signal of cells coexpressing the LRS/tRNALeu pair in the presence or absence of **1**. Data from two independent biological replicates (unpaired *t* test; **: $p \leq 0.01$). (d) FCM-based monitoring of 5hmC and expression of hTET1CD constructs (by mCherry): gray, standard transfection of amber-free wt hTET1CD; black, cotransfection of vectors encoding hTET1CD-S2045 → TAG and the (LRS)/tRNALeu pair grown in the presence of **1** with light irradiation after 24 h; white, without light irradiation (in all cases cotransfected with the EGFP-only control). Upper panel shows mean 5hmC intensities selected for a medium TET1 expression group (cell numbers are 30, 42, and 48 for t = 6, 8, and 10 h, respectively; cell numbers are >1000 for all other time points). Lower panel shows hTET1CD expression as % mCherry-positive cells. Error bars are from standard error of the mean (SEM) of at least three independent biological replicates.

formation is not recorded in a window of increasing TET1 levels that would prevent correct kinetic measurements (Figure 3d lower panel, black and white bars). In contrast, a reference experiment without light control-employing cells transfected only with a vector encoding the amber-free wt hTET1CD showed a slow and nonlinear increase of 5hmC over 20 h. In this window, also the (rate-limiting) hTET1CD levels increased strongly with a marked leap at 12 h, illustrating the difficulty of measuring the correct TET1 kinetics without temporal control of the catalytic activity (Figure 3d, gray triangles and bars). As further basic controls, we conducted experiments with or without RNase A treatment that confirmed that the 5hmC signal observed in our assay was due to 5mC oxidation in DNA and not RNA (Figure S9). Moreover, the 5hmC signals for the 2 h time points of this and

https://doi.org/10.1021/acschembio.2c00245
ACS Chem. Biol. 2022, 17, 1844−1852

selected later experiments observed by FCM correlated with the results of dot blot assays using the same 5hmC antibody (Figure S10).

With our new tool in hand, we aimed to study the modulation of hTET1CD-catalyzed 5hmC formation by full-length wt hMBD1 (Figure 4a) on the kinetic level. We initially evaluated the ability of wt hMBD1 to bind mCpGs by imaging in mouse fibroblast NIH/3T3 cells. In these cells, pericentromeric heterochromatin is highly enriched in 5mC and forms characteristic chromocenters that are stained by functional, fluorescently labeled MBDs and DNA stains such as DAPI.[2,3] Colocalization of wt hMBD1 and DAPI confirmed mCpG binding (Figure 4b; see Figure S11 for additional images).

We cotransfected HEK293T cells with vectors encoding hTET1CD-S2045 → TAG and the (LRS)/tRNA^{Leu} pair and with a third vector encoding either EGFP-tagged hMBD1 (Figure 4a) or EGFP only. We then monitored the TET1-mediated 5hmC formation over a window of 8 h after light irradiation, this time for different groups of MBD/TET expression ratios (Figure 4c). In the presence of MBD1, 5hmC was downregulated over the whole time window compared to the EGFP control (Figure 4d). This effect was dose dependent with respect to the wt hMBD1 expression level (Figures 4e and S3). Given the affinity of both MBD1 and TET1 for mCpGs, this result can be explained by a reduction of available mCpG substrate for TET1 by the competing MBD1. To test this hypothesis, we constructed two additional MBD1 mutants: one R22C+R44C mutant and one ΔMBD variant missing the complete MBD domain (MBD1−ΔMBD, Figure 4f). These mutants have been reported to not bind mCpG anymore, and we confirmed that they do not colocalize with DAPI in the chromocenter assay (Figure 4g).[22] In subsequent kinetic measurements, MBD1-R22C+R44C indeed did not downregulate 5hmC formation, supporting our hypothesis. Instead, we surprisingly found that the 5hmC formation was slightly enhanced in the first 2 h after light activation and reached a saturation 4 h after activation (Figure 4h). We again analyzed three expression groups as above (Figure 4c). This analysis again showed an upregulation of 5hmC by hMBD1-R22C+R44C over the first 2 h that was dose dependent at 0.5 h, whereas the EGFP-only control did not show any dose-dependent effect (Figure 4i; see Figure S3 for the 2 h time point). It is to be noted that the coexpression of hMBD1 or its variants did not affect the cellular 5hmC level in the absence of light irradiation, showing that the 5hmC formation is strictly controlled by light activation of hTET1CD-S2045 → **1** (Figure S8). In addition, we did not observe differences in hmC formation for MBD1-expressing cells sorted for the N-terminal Flag tag of hTET1 as compared to cells sorted for the hTET1 C-terminal mCherry tag. This suggests that the expression of C-terminally truncated hTET1 (i.e., amber termination products) does no influence the kinetics of the correct, amber suppressed hTET1, e.g., via interactions with MBD1 (Figure S12).

Interestingly, the presence of the MBD1−ΔMBD variant did not result in an increased 5hmC formation kinetics, which on one hand further substantiates the model of direct competition between the MBD domain and TET1 at mCpGs but on the other hand implies that the MBD domain as a whole has a function in the observed TET1 activation by hMBD1-R22C +R44C (Figure 4h,i).

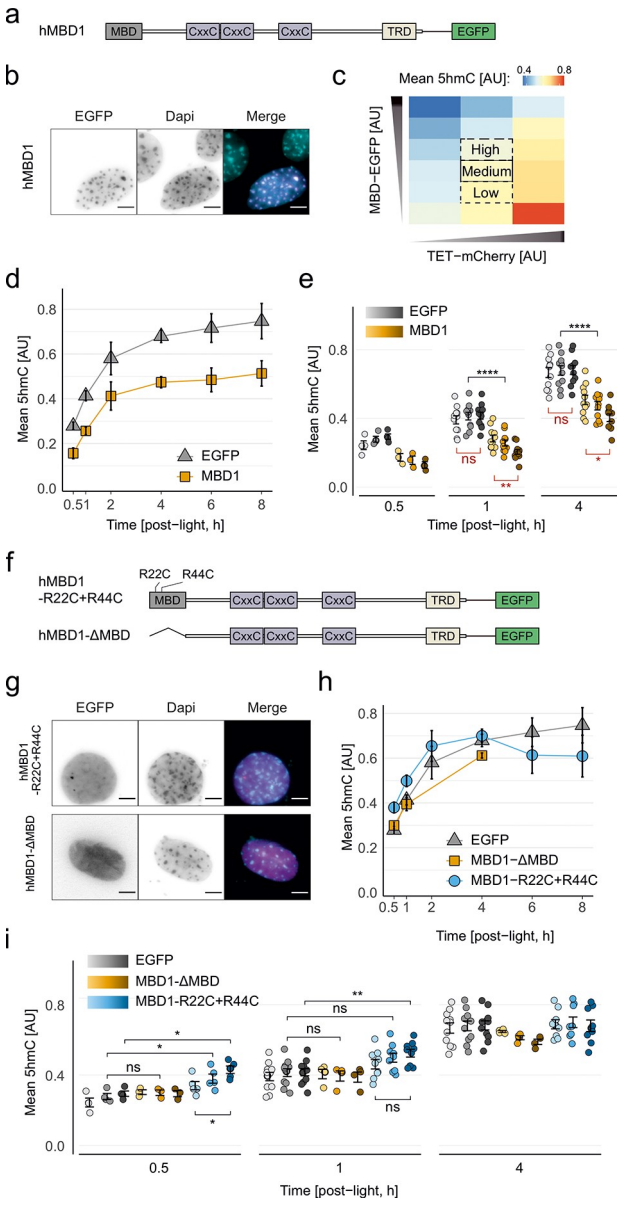

Figure 4. Kinetic measurements of TET1 activity and its modulation by MBD1. (a) Domain structures of hMBD1 tagged with C-terminal EGFP. (b) Imaging of wt hMBD1 in NIH/3T3 cells. Foci in DAPI staining indicate the mCpG-rich chromocenters; the merged image shows the colocalization of hMBD1 (blue) and DAPI foci (cyan). Scale bar: 5 μm. (c) Protein expression groups selected for 5hmC analyses shown as a 5hmC heat map of one exemplary experiment. (d) Kinetic measurements of hTET1CD-S2045 → **1**-mediated 5hmC formation in HEK293T cells coexpressing wt hMBD1 or EGFP only. Mean global 5hmC intensities from >100 cells in the medium MBD/TET expression group are plotted; error bars are from SEM of at least three independent biological replicates. (e) Dose-dependent analysis from three different MBD/TET expression groups (gradient bar, from left to right: low, medium, high) at selected time points. Mean 5hmC intensities from at least three independent biological replicates. The p values from the Mann−Whitney test are indicated (*: $p \leq 0.05$; **: $p \leq 0.01$; ****: $p \leq 0.0001$; ns: $p > 0.05$). (f) Domain structures of hMBD1 R22C+R44C and ΔMBD mutants tagged with C-terminal EGFP. (g) Imaging of hMBD1 R22C+R44C and ΔMBD mutants in NIH/3T3 cells as in (b). Scale bar: 5 μm. (h) Kinetic measurements of TET1-mediated 5hmC formation in HEK293T cells coexpressing hMBD1-R22C+R44C, hMBD1−ΔMBD, or EGFP only. Mean 5hmC intensities from cell populations (>100 cells) in the medium MBD/

https://doi.org/10.1021/acschembio.2c00245
ACS Chem. Biol. 2022, 17, 1844−1852

Figure 4. continued

TET ratio group are plotted; error bars indicate SEM from at least 3 independent biological replicates. (i) Dose-dependent analysis from three different MBD/TET ratios (gradient bar, from left to right: low, medium, high) at selected time points. Mean 5hmC intensities from >3 independent biological replicates were plotted. The p values from the Mann−Whitney test are indicated (*: $p \leq 0.05$; **: $p \leq 0.01$; ns: $p > 0.05$).

Overall, these results indicate that the competition for mCpGs by a functional MBD domain might not be the only factor in the modulation of TET1 activity by MBD1.

2.3. Kinetic Studies Hint at a Role of the CXXC3 Domain in Promoting TET1 Activity. To get insights into the regulatory roles of additional hMBD1 domains, we first investigated the role of the third CXXC (CXXC3) domain that is known to selectively bind to unmethylated CpGs.[23] We constructed two CXXC3 variants of hMBD1 either by cloning a natural hMBD1 isoform that lacks the complete CXXC3 domain (isoform 7, MBD1v7; Figure 5a)[24] or by mutating two cysteine residues responsible for Zn(II) binding and CpG affinity (C338A+C341A[12,25]). In imaging experiments, both variants behaved like wt hMBD1 and bound to chromocenters in NIH/3T3 cells (Figure 5b). Moreover, coexpression of both variants led to a similar reduction of TET1 kinetics in FCM analyses as wt hMBD1 (Figure 5c; see Figure S4 for dose dependence).

To study the role of the CXXC3 domain independently from the competing effect of the MBD domain, we next introduced R22C+R44C mutations into the two hMBD1 variants in order to remove the mCpG affinity of the MBD (Figure 5d). Neither of the two hMBD1 variants bound chromocenters in NIH/3T3 cells (Figure 5e). In contrast to the R22C+R44C mutant, they predominantly located to nucleoli, suggesting a role of the CXXC3 domain in localizing hMBD1 to other areas of the nucleus (Figures 5e and S5). Interestingly, both variants showed virtually identical kinetics as the EGFP-only control and did not exhibit a dose-dependent upregulation of TET1 kinetics as for the MBD1-R22C+R44C mutant with functional CXXC3 (Figures 5f and S6). This data implies a role of interactions between nonmethylated CpG and the CXXC3 domain in the upregulation of TET1 activity.

Interestingly, a previous imaging study showed a recruitment of mouse TET1 to pericentromeric heterochromatin in mouse fibroblasts by mouse MBD1 that also depended on a functional CXXC3 domain and resulted in an increased oxidation of local 5mC.[7] Moreover, coimmunoprecipitation (co-IP) experiments with mTET1 and different domain truncation variants of mMBD1 showed an interaction between the two proteins. Whereas these experiments suggested an interaction involving multiple mMBD1 domains, truncation of the MBD domain itself resulted in a reduced co-IP. This data is in agreement with our finding that the hMBD1−ΔMBD variant did not show an upregulation of TET1 activity.

2.4. Evaluation of the TRD Domain in the Regulation of TET1 Activity. Finally, we were interested in the role of the transcriptional repressor domain (TRD) of hMBD1. The TRD has been shown to interact with multiple chromatin factors to mediate condensation and transcriptional silencing, such as the histone−lysine methyltransferases SETDB1 as well as the MBD1 chromatin associated factor 1 (MCAF1).[26−29] Hence,

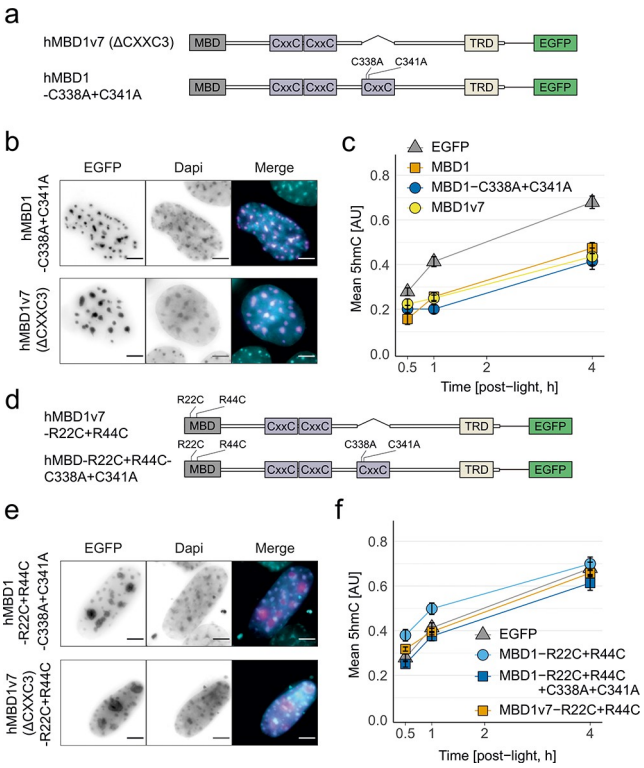

Figure 5. Role of the CXXC3 domain of hMBD1 in the modulation of TET1 activity. (a) Domain structures of hMBD1 CXXC3 mutants (isoform 7 and C338A+C341) tagged with C-terminal EGFP. (b) Imaging of hMBD1 CXXC3 mutants (isoform 7 and C338A+C341) in NIH/3T3 cells as in Figure 4b. Scale bar: 5 μm. (c) Kinetic measurements of 5hmC formation in HEK293T cells coexpressing hTET1CD-S2045 → 1 and an hMBD1 CXXC3 mutant (isoform 7 and C338A+C341), wt hMBD1, or EGFP only. Mean global 5hmC intensities are from >100 cells in the medium MBD/TET expression group; error bars indicate SEM from at least three independent biological replicates. (d) Domain structures of hMBD1 mutants (isoform7-R22C+R44C and R22C+R44C+C338A+C341) tagged with C-terminal EGFP. (e) Imaging of hMBD1 mutants (isoform 7-R22C+R44C and R22C+R44C+C338A+C341) in DAPI-stained NIH/3T3 cells as in Figure 4b. Scale bar: 5 μm. (f) Kinetic measurements of the 5hmC formation in HEK293T cells coexpressing hTET1CD-S2045 → 1 and hMBD1 mutants (R22C+R44C, R22C +R44C+C338A+C341A, isoform7-R22C+R44C) or EGFP only. Mean global 5hmC intensities are from >100 cells of the medium MBD/TET expression group; error bars show SEM from at least three independent biological replicates.

the TRD may mediate condensation and reduced DNA accessibility and thus downregulate TET1 kinetics in addition to the direct competition with the MBD domain. We performed kinetic measurements with an hMBD1 isoform lacking the TRD (MBD1-ΔTRD, Figure 6a) that exhibited chromocenter localization as expected (Figure 6b). This variant downregulated TET1 kinetics to a similar extent and with similar dose dependence as wt hMBD1 (Figures 6c and S7), suggesting that the effects of TRD-mediated condensation are either masked by the direct competition of the MBD or that they are not yet coming into play within our observation time window. Interestingly, co-IP experiments have shown that a short C-terminal fragment of mMBD1 containing the TRD is able to interact with mTET1.[12] Thus, we were interested in determining if this interaction was required for the observed TET1 activation based on a functional CXXC3. We conducted

https://doi.org/10.1021/acschembio.2c00245
ACS Chem. Biol. 2022, 17, 1844−1852

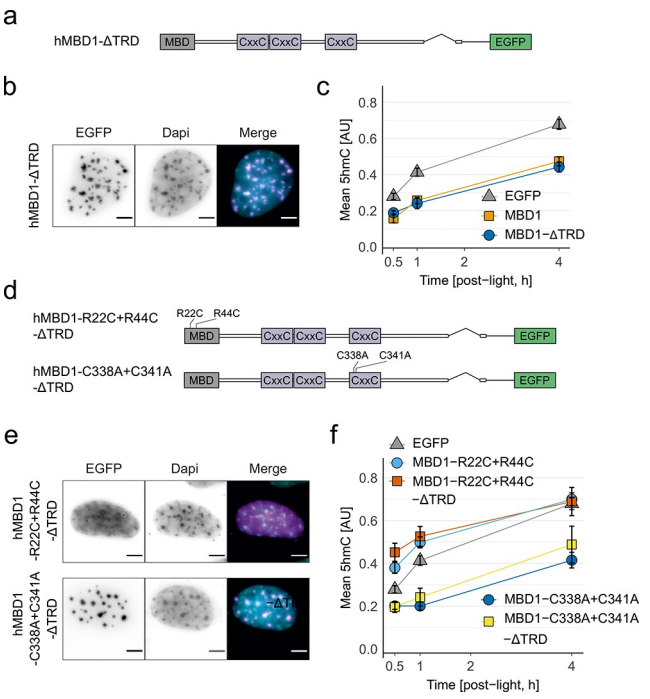

Figure 6. Role of the TRD domain of hMBD1 in the modulation of TET1 activity. (a) Domain structure of the hMBD1-ΔTRD mutant tagged with C-terminal EGFP. (b) Imaging of hMBD1-ΔTRD in NIH/3T3 cells as in Figure 4b. Scale bar: 5 μm. (c) Kinetic measurements of the hTET1CD-S2045 → **1**-mediated 5hmC formation in HEK293T cells coexpressing hMBD1-ΔTRD, wt hMBD1, or EGFP only. Mean global 5hmC intensities from cell populations (>100 cells) in the medium MBD/TET ratio group are plotted; error bars indicate SEM from more than three independent biological replicates. (d) Domain structures of hMBD1 ΔTRD mutants (R22C+R44C-ΔTRD and C338A+C341A-ΔTRD) tagged with C-terminal EGFP. (e) Imaging of hMBD1 ΔTRD mutants (R22C+R44C-ΔTRD and C338A+C341A-ΔTRD) in NIH/3T3 cells as in Figure 4b. Scale bar: 5 μm. (f) Kinetic measurements of hTET1CD-S2045 → **1**-mediated 5hmC formation in HEK293T cells coexpressing hMBD1 ΔTRD mutants (R22C+R44C-ΔTRD and C338A+C341A-ΔTRD), R22C+R44C mutant, C338A+C341A mutant, or EGFP only. Mean global 5hmC intensities from cell populations (>100 cells) in the medium MBD/TET ratio group are plotted; error bars indicate SEM from more than three independent biological replicates.

experiments with the same hMBD1-ΔTRD variant but with added R22C+R44C or C338A+C341A mutations (Figure 6d) and compared them to the same variants with the TRD (as expected, only the latter mutant showed chromocenter binding; Figure 6e). Both C338A+C341A mutants showed a similar inhibition of TET1, i.e., independently of the presence or absence of the TRD (Figures 6f and S7). In contrast, the R22C+R44C mutants showed the expected activation but again without a significant difference between the two variants (Figures 6f and S7). This data suggests either that the TRD of hMBD1 does not interact with hTET1 in the same way as observed for the murine proteins or that this interaction does not additionally contribute to CXXC3-dependent activation of hTET1.

3. CONCLUSION

5mC is the central regulatory element of mammalian DNA and is critically involved in the shaping of cellular phenotypes. Key to this process is the dynamic editing and interpretation of 5mC by TET dioxygenases and MBD proteins. We here aimed to study the interplay between human TET1 and MBD readers at their common mCpG substrate via in vivo kinetic measurements of TET-catalyzed 5mC oxidation kinetics. In a coexpression screen with hTET1 and the five core family hMBD proteins based on FCM analyses of hTET1-mediated 5hmC formation, we identified hMBD1 as a negative regulator of hTET1. We then employed light activation of TET dioxygenases via a genetically encoded photocaged serine, enabling tight temporal control of TET1 catalysis. This enables the uncoupling of the TET1 oxidation kinetics from the kinetics of processes that occur upstream, such as TET1 and MBD translation, post-translational modification, and localization.

We found that the presence of a functional MBD domain in hMBD1 reduces the rate of 5mC oxidation by hTET1, which can be explained by a competition and masking of mCpG by hMBD1 and thus reduction of available substrate for hTET1. The effect was independent of the presence of the CXXC3 domain or its ability to bind nonmethylated CpG. Intriguingly, hMBD1 with a functional CXXC3 domain and an MBD domain that was not able to bind mCpGs increased the oxidation kinetics of TET1. This hints at a secondary function of hMBD1 in its interplay with TET1 that in our model is obscured by the dominant downregulating effect of the MBD domain itself. This upregulation is dependent on the presence of the MBD domain as a whole, which suggests a general involvement of the domain in this second regulatory function. A previous study carried out with the murine proteins in mouse fibroblasts without light control did not report a downregulation of oxidation but instead revealed an mMBD1-CXXC3-dependent localization of mTET1 to pericentromeric heterochromatin, together with an increased 5hmC formation.[12] Co-IP experiments further revealed a direct interaction between mMBD1 and mTET1 that involved the MBD domain. Though we observe a CXXC3-dependent upregulation of the oxidation rate only if the MBD domain is unable to bind mCpG, our data is nevertheless in agreement with such a CXXC3-dependent recruitment of TET1 to CpG and an associated increase of mCpG oxidation (Figure 7).[12] Given that CpGs are the ultimate product of TET-mediated oxidation and active demethylation of mCpGs, this activation is reminiscent of reader-editor cross-talk known for other chromatin proteins. Full-length hTET1 itself also carries an N-terminal CXXC domain that preferentially binds to

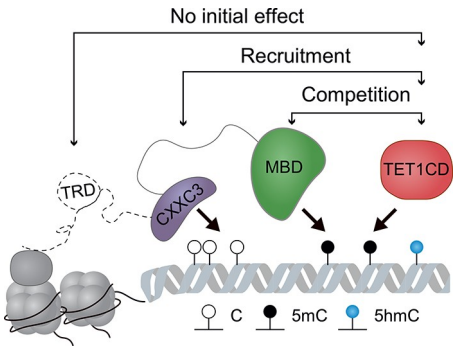

Figure 7. Model for the domain-dependent interplay between MBD1 and TET1 leading to a dual regulation of 5mC oxidation by TET1 via MBD1.

https://doi.org/10.1021/acschembio.2c00245
ACS Chem. Biol. 2022, 17, 1844−1852

unmethylated CpGs and may provide an additional editor-product crosstalk.[3] This aspect is not covered by our study employing the catalytic domain of hTET1. However, full-length hTET1 and its catalytic domain showed a similar behavior with respect to their interplay with MBD1 in a previous imaging-based chromocenter study.[12] In contrast, we did not observe differences in the regulation for MBD1 variants with or without the TRD domain, which has also been shown to interact with TET1 for the murine proteins. These results indicate that a potential TRD-mediated chromatin condensation does not play a role for TET1 regulation in our model and observation time window and that a potential TRD-mediated interaction with hTET1 does not further increase the observed CXXC3-dependent activation. Overall, we envision that our light-activation approach can be more broadly applied for the study of the regulation of TET kinetics by other chromatin factors to reveal their involvement in normal and disease processes.

4. METHODS

4.1. Construction of Plasmids for MBD and TET Protein Expression. All vectors were derived from pShP2384, which is based on pcDNA3.1-GoldenGate-VP64 (Addgene 47389) with removed VP64 and lacZα gene as described previously.[13] The mCherry transfection control on pShP2384 was deleted using whole plasmid PCR and religation with primers o3246/o3247 resulting in plasmid pTzL1744. Then, the mCherry sequence amplified with primers o3254/o3255 was inserted into pTzL1744 (amplified with primers o3256/o3257) via Gibson assembly, followed by quick change site-directed mutagenesis (SDM) to correct a frameshift using primers o3284/o3285 (yielding plasmid pTzL1745).

To construct plasmids encoding EGFP-tagged hMBD1, a Myc tag was first introduced into pTzL1745 by quick change SDM using primers o3167/o3257, resulting in pTzL1746. The human full length MBD1 coding sequence was amplified from a human prostate cDNA library (BiocCt 10108-A-GVO-EB) using primers o3292/o3293; then, MBD1 and EGFP (amplified with primers o3294/o3295) were assembled with pTzL1746 (amplified by primers o3290/o3291) via Gibson assembly, yielding pTzL1747. Finally, the remaining unwanted sequences were removed by quick change using primers o3642/o3643, yielding pTzL1836.

The EGFP-tagged hMBD1 mutants were cloned as follows. The R22C mutation was introduced into pTzL1836 by quick change SDM using primers o3730/o3731 to yield pTzL1947. The R22C+R44C mutant was derived from pTzL1947 by introducing an R44C mutation with primers o3732/o3733 via quick change SDM to yield pTzL1964. The C338A+C341A mutations were introduced into pTzL1836 (hMBD1) and pTzL1964 (hMBD1-R22C+R44C) using primers o4479/o4480, resulting in pTzL2645 and pTzL2646, respectively. The hMBD1-dMBD (aa 1−69 deleted) variant was cloned by Gibson assembly of a truncated hMBD1 sequence (amplified with primers o3293/o4300) and the pTzL1836 backbone (amplified with primers o3386/o3291), yielding pBiR2585. The hMBD1-dTRD (aa 529−592 deleted) variant was cloned by the Gibson assembly of 2 fragments amplified from pTzL1836 using primers o4302/o3291 and o3292/o4305, yielding pBiR2586. The hMBD1 isoform 7 (hMBD1v7, aa 327−382 deleted from isoform 1 sequence) variant was cloned by the Gibson assembly of 3 fragments amplified from pTzL1836 using primers o3292/o4189, o4298/o3293, and o3386/o3291, yielding pBiR2593. The hMBD1v7-R22C+R44C variant was cloned by the Gibson assembly of 3 fragments amplified from pTzL1964 using primers o3292/o4189, o4298/o3293, and o3386/o3291, yielding pBiR2628. For EGFP-tagged hMBD3, the human MBD3 isoform 2 (MBD3v2) coding sequence was first amplified from human prostate cDNA using primers o3380/o3381 and inserted in the vector backbone of pTzL1747 (amplified by primers o3386/o3291) via the Gibson assembly, resulting in pTzL1774. Unwanted sequences were subsequently removed by quick change SDM using primers o3642/o3643 giving pTzL1835. Finally, the canonical human MBD3 sequence (isoform 1) was cloned by inserting the coding sequence of MBD3 aa 5−36 into pTzL1835 via quick change SDM using primers o3810/o3811. For EGFP-tagged hMBD2a, the coding sequence for human MBD2a was amplified from a plasmid encoding human full length MBD2a (Addgene 78141) using primers o3510/o3511 and then inserted into the backbone of pTzL1835 (amplified by primers o3386/o3291) via the Gibson assembly, resulting in pTzL1889. For EGFP-tagged hMBD4, the coding sequence for human MBD4 was amplified from human prostate cDNA using primers o3382/o3383 and then inserted into the backbone of pTzL1835 (amplified by primers o3386/o3291) via the Gibson assembly, followed by frameshift correction with primers o3758/o3759 to yield pTzL1948. For EGFP-tagged hMeCP2, the coding sequence for human MeCP2 was amplified from human prostate cDNA using primers o3384/o3385 and inserted into the backbone of pTzL1747 via restriction ligation using *Asc*I/*Kpn*I, resulting in pTzL1773. Unwanted sequences were subsequently removed by quick change SDM using primers o3642/o3643 to afford pTzL1834. For the expression vector encoding EGFP only, the hMBD1 sequence in pTzL1836 was replaced with a $(GGGGS)_3$ linker by restriction/ligation of annealed oligos o3825/o3826 and the pTzL1836 backbone using *Asc*I/*Kpn*I, resulting in pTzL1990.

For mCherry-tagged hTET1CD (aa 1418−2136), the coding sequence for the human TET1 catalytic domain was amplified from a plasmid encoding human full length TET1 (Addgene 49792) using primers o3751/o3473 and then assembled with 2 vector backbone fragments of pTzL1837 (cloned from pTzL1745 by deleting unwanted sequences with primers o3642/o3643) amplified with primers o2261/o3596 and o3288/o2260, resulting in plasmid pTzL1960. The mutations (H1672Y, D1674A) that remove catalytic activity were introduced into hTET1CD plasmid (pTzL1960) using o3762/o3763, resulting in pTzL1970. The plasmid encoding amber mutant hTET1CD-S2045^{TAG} was cloned by restriction ligation of the hTET1CD-S2045^{TAG} sequence (digested from pShP2444) and vector backbone of pTzL1960 using *Asc*I/*Kpn*I, yielding pTzL2504. Another hTET1CD-S2045^{TAG} plasmid bearing additional N-terminal Flag tags and the GGGGS linker was cloned by restriction ligation of the hTET1CD-S2045^{TAG} sequence with the vector backbone of pTzL1833 using *Asc*I/*Xba*I, giving plasmid pTzL2513.

The orthogonal *E. coli* leucyl synthetase (ecLRS-BH5) bearing the five previously reported mutations M40G, L41Q, Y499L, Y527G, and H537F2 and the suppressor tRNA^{CUA} were encoded on the previously reported plasmid pStH1147.[13]

4.2. Cell Culture. HEK293T cells were cultivated in DMEM (Dulbecco's Modified Eagle Medium) supplemented with 10% FBS, 2 mM L-glutamine, 100 U/mL penicillin, and 0.1 mg mL^{-1} streptomycin in a sterile humidified incubator (≥95%) at 37 °C and a CO_2 level of 5%. For transfection, cells were seeded a day before to reach 70−80% confluency at the time of transfection. Transient plasmid transfection was carried out by the use of polyethylenimine (PEI; 1 mg mL^{-1} in dd H_2O, pH 7) (linear MW 25 000 g/mol, CAS 9002-98-6, Alfa Aesar). Mouse embryonic fibroblast NIH/3T3 cells (ATCC, CRL-1658) were maintained in the same conditions described above. The plasmid transfection of NIH/3T3 was done either by PEI as described above or by electroporation using the 10 μL Neon Transfection System (Invitrogen, Thermo Fisher Scientific Inc.). Briefly, 50 000 cells were resuspended in 10 μL of resuspension buffer R with 0.25 μg of plasmid and electroporated at a pulse voltage of 1400 V, pulse width of 20 ms, and pulse number of 2. The cells were subsequently seeded in a 96-well plate containing DMEM supplemented with 10% FBS and 2 mM L-glutamine and then left to adhere in a humidified 37 °C incubator with 5% CO_2.

4.3. Light Activation of TET1. HEK293T cells grown in 6-well cell culture plate (Sarstedt) were transfected with plasmids encoding TET1CD-S2045^{TAG}, LeuRS/tRNA^{Leu}, and the desired MBD proteins. At 3 h post-transfection, growth media was exchanged with media supplemented with 0.05 mM **1** (TOCRIS, 780009-55-4) and allowed to express for 24 h. For light treatment, growth media containing **1** was replaced by warm DPBS (Dulbecco's phosphate-buffered saline,

https://doi.org/10.1021/acschembio.2c00245
ACS Chem. Biol. 2022, 17, 1844−1852

Mg/Ca free) and subsequently placed on a 365 nm UV transilluminator (Witeg DH.WUV00010, 6×, 15 W) for 3 min. Immediately after irradiation, DPBS was replaced by preheated growth media (without **1**), and cells were maintained in a humidified 37 °C incubator with 5% CO_2 until harvesting.

4.4. Fluorescence Microscopy and Image Analysis. NIH/3T3 cells transfected by PEI or electroporation were grown in black 96-well plates with a flat polymer coverslip bottom (ibidi, 89626). After the protein of interest was stably expressed (16−24 h), cells were fixed with 4% formaldehyde for 10−15 min at RT followed by three DPBS washes. Fixed cells were subjected to permeabilization using 0.25% Triton X-100 for 15−20 min at RT. After three DPBS rinses, nuclei were stained with 1 μg/mL DAPI in DPBS for 5 min in the dark and directly imaged. Experiments were performed using an Olympus IX81 microscope equipped with LEDs as the excitation light source (150−750 mW) and coupled with a Hamamatsu model C10600-10B-H camera. Images were acquired using a 100× oil immersion objective and *z*-stack images (0.5 μm/step) for EGFP (excitation filter 475/28 nm, emission filter 554/23 nm), mCherry (excitation filter 555/28 nm, emission filter 635/18 nm), and DAPI (excitation filter 395/25 nm, emission filter 474/27 nm). The intensity and subcellular localization of foci were analyzed from *z*-projections of image stacks with maximal intensity (1344 × 1024 pixels, 32 bits) using ImageJ 1.[30]

4.5. Immunostaining and Flow Cytometry. Cells trypsinized at desired time points after transfection or light activation (described above) were placed in 5 mL round-bottom polystyrene tubes (Falcon, 352058) and washed once with DPBS. After collection by centrifugation, cells were fixed with medium A (Fix & Perm cell permeabilization kit, Thermo Scientific, GAS004) for 15 min at RT and subsequently washed with wash buffer (DPBS with 5% FBS). Then, the fixed cells were permeabilized with medium B (Fix & Perm kit) for 20 min. In control experiments with or without RNase A treatment, an additional incubation step with RNase A (10 μg/mL in DPBS, Qiagen, 19101) at 37 °C for 30 min was added after permeabilization. Thereafter, cells were resuspended in 2 N HCl and incubated for 30 min at RT to denature chromosomal DNA, immediately followed by dilution to a final concentration of 0.4 N HCl with DPBS. The HCl solution was removed by centrifugation, and the cell pellet was washed with wash buffer. Before immunostaining, cells were resuspended in blocking buffer (DPBS with 1% BSA and 0.05% Tween 20) and incubated for 1 h at RT or overnight at 4 °C with gentle shaking. To detect genomic 5hmC, a rabbit anti-5hmC (Active Motif, 39769) primary antibody and Alexa Fluor 405-conjugated goat antirabbit (Invitrogen, A-31556) secondary antibody were used. Cells were incubated with anti-5hmC antibody (1:1000) and 1% BSA in 1× intracellular staining buffer (SONY, 2705010) for 1 h followed by three washing steps with PBST buffer (DPBS with 0.05% Tween 20). Then, cells were incubated with AF405-conjugated secondary antibody (1:1000) and 1% BSA in intracellular staining buffer for 1 h. After three washing steps with PBST buffer, cells were resuspended in DSPBS and subjected to a cell strainer (Falcon, 352235) for FCM measurement. FCM measurements were performed with a Sony Cell Sorter model LE-SH800SFP using 405, 488, and 561 nm lasers coupled with 450/50 nm (FL1), 525/50 nm (FL2) and 600/60 nm (FL3) filters to detect AF405, EGFP, and mCherry, respectively. FCM results were exported as flow cytometry standard files (FCS 3.0 or 3.1) by the cell sorter software (v. 2.1.3 or v. 2.1.5, Sony Biotechnology) and analyzed using R as described below.

4.6. FCM Data Analysis by R. Flow cytometry standard files (FCS 3.0 or 3.1) were processed with R 4.0.0 in Rstudio (Version 1.2.5042) using the following Bioconductor packages: flowCore (2.0.0),[31] flowClust (3.26.0),[32,33] flowDensity (1.22.0),[34] flowStats (4.0.0),[35] and ggcyto (1.16.0).[36] Fluorescence intensity data extracted from populations of interest were then analyzed using Tidyverse packages (1.3.0). In brief, cell populations were identified first from multivariate t mixture models; then, singlet events were selected by a robust linear model with *rlm*. Populations showing positive or negative fluorescence signals were further separated by applying thresholds identified from the respective negative controls (the upper boundary including 99.9% population in respective channels accordingly to the density distribution). The gated positive population of the individual sample was further grouped by their MBD(EGFP) and TET(mCherry) intensities, and the median AF405 intensity (5hmC) of each group was normalized to that of the gated negative population from the same sample (Figure S1).

■ ASSOCIATED CONTENT

Supporting Information

The Supporting Information is available free of charge at https://pubs.acs.org/doi/10.1021/acschembio.2c00245.

Oligonucleotide and protein sequences, data of imaging experiments, FCM, and biochemical assays, additional methods, and plasma maps (PDF)

■ AUTHOR INFORMATION

Corresponding Author

Daniel Summerer − *Department of Chemistry and Chemical Biology, Technical University of Dortmund, 44227 Dortmund, Germany;* orcid.org/0000-0002-3019-7241; Email: Daniel.Summerer@tu-dortmund.de

Authors

Tzu-Chen Lin − *Department of Chemistry and Chemical Biology, Technical University of Dortmund, 44227 Dortmund, Germany*

Shubhendu Palei − *Department of Chemistry and Chemical Biology, Technical University of Dortmund, 44227 Dortmund, Germany;* orcid.org/0000-0003-4447-7022

Complete contact information is available at: https://pubs.acs.org/10.1021/acschembio.2c00245

Funding

This work has received funding from the European Research Council (ERC) under the ERC consolidator grant EPICODE, No. 723863.

Notes

The authors declare no competing financial interest.

■ ACKNOWLEDGMENTS

We acknowledge the Faculty of Chemistry and Chemical Biology of the TU Dortmund University and the International Max-Planck Research School in Chemical and Molecular Biology/Living Matters for continuous support. We thank H. Schwarzenbach for plasmid MBD2a pcDNA3.1, A. Rao for plasmid FH-TET1-pEF, and C. Gersbach for plasmid pcDNA3.1-GoldenGate-VP64 obtained via Addgene.

■ REFERENCES

(1) Allis, C. D.; Jenuwein, T. The molecular hallmarks of epigenetic control. *Nat. Rev. Genet.* **2016**, *17*, 487−500.

(2) Wu, X.; Zhang, Y. TET-mediated active DNA demethylation: mechanism, function and beyond. *Nat. Rev. Genet* **2017**, *18*, 517.

(3) Du, Q.; Luu, P. L.; Stirzaker, C.; Clark, S. J. Methyl-CpG-binding domain proteins: readers of the epigenome. *Epigenomics* **2015**, *7*, 1051−1073.

(4) Carell, T.; Kurz, M. Q.; Muller, M.; Rossa, M.; Spada, F. Non-canonical Bases in the Genome: The Regulatory Information Layer in DNA. *Angew. Chem., Int. Ed. Engl.* **2018**, *57*, 4296−4312.

(5) Spruijt, C. G.; Gnerlich, F.; Smits, A. H.; Pfaffeneder, T.; Jansen, P. W.; Bauer, C.; Munzel, M.; Wagner, M.; Muller, M. Khan; et al. Dynamic readers for 5-(hydroxy)methylcytosine and its oxidized derivatives. *Cell* **2013**, *152*, 1146−1159.

(6) Hashimoto, H.; Olanrewaju, Y. O.; Zheng, Y.; Wilson, G. G.; Zhang, X.; Cheng, X. Wilms tumor protein recognizes 5-carboxylcytosine within a specific DNA sequence. *Genes Dev.* **2014**, *28*, 2304−2313.
(7) Kellinger, M. W.; Song, C. X.; Chong, J.; Lu, X. Y.; He, C.; Wang, D. 5-formylcytosine and 5-carboxylcytosine reduce the rate and substrate specificity of RNA polymerase II transcription. *Nat. Struct. Mol. Biol.* **2012**, *19*, 831−833.
(8) Raiber, E. A.; Portella, G.; Martinez Cuesta, S.; Hardisty, R.; Murat, P.; Li, Z.; Iurlaro, M.; Dean, W.; Spindel, J.; Beraldi, D.; et al. 5-Formylcytosine organizes nucleosomes and forms Schiff base interactions with histones in mouse embryonic stem cells. *Nat. Chem.* **2018**, *10*, 1258−1266.
(9) Pfeifer, G. P.; Szabo, P. E.; Song, J. Protein Interactions at Oxidized 5-Methylcytosine Bases. *J. Mol. Biol.* **2019**, *19*, 30501−30507.
(10) Rausch, C.; Hastert, F. D.; Cardoso, M. C. DNA Modification Readers and Writers and Their Interplay. *J. Mol. Biol.* **2020**, *432*, 1731−1746.
(11) Ludwig, A. K.; Zhang, P.; Hastert, F. D.; Meyer, S.; Rausch, C.; Herce, H. D.; Muller, U.; Lehmkuhl, A.; Hellmann, I.; Trummer, C.; et al. Binding of MBD proteins to DNA blocks Tet1 function thereby modulating transcriptional noise. *Nucleic Acids Res.* **2017**, *45*, 2438−2457.
(12) Zhang, P.; Rausch, C.; Hastert, F. D.; Boneva, B.; Filatova, A.; Patil, S. J.; Nuber, U. A.; Gao, Y.; Zhao, X.; Cardoso, M. C. Methyl-CpG binding domain protein 1 regulates localization and activity of Tet1 in a CXXC3 domain-dependent manner. *Nucleic Acids Res.* **2017**, *45*, 7118−7136.
(13) Palei, S.; Buchmuller, B.; Wolffgramm, J.; Munoz-Lopez, A.; Jung, S.; Czodrowski, P.; Summerer, D. Light-Activatable TET-Dioxygenases Reveal Dynamics of 5-Methylcytosine Oxidation and Transcriptome Reorganization. *J. Am. Chem. Soc.* **2020**, *142*, 7289−7294.
(14) Zhang, P.; Ludwig, A. K.; Hastert, F. D.; Rausch, C.; Lehmkuhl, A.; Hellmann, I.; Smets, M.; Leonhardt, H.; Cardoso, M. C. L1 retrotransposition is activated by Ten-eleven-translocation protein 1 and repressed by methyl-CpG binding proteins. *Nucleus-Phila* **2017**, *8*, 548−562.
(15) Peng, L.; Li, Y.; Xi, Y.; Li, W.; Li, J.; Lv, R.; Zhang, L.; Zou, Q.; Dong, S.; et al. MBD3L2 promotes Tet2 enzymatic activity for mediating 5-methylcytosine oxidation. *J. Cell. Sci.* **2016**, *129*, 1059−1071.
(16) Cartron, P. F.; Nadaradjane, A.; Lepape, F.; Lalier, L.; Gardie, B.; Vallette, F. M. Identification of TET1 Partners That Control Its DNA-Demethylating Function. *Genes Cancer* **2013**, *4*, 235−241.
(17) Hu, L.; Li, Z.; Cheng, J.; Rao, Q.; Gong, W.; Liu, M.; Shi, Y. G.; Zhu, J.; Wang, P.; Xu, Y. Crystal structure of TET2-DNA complex: insight into TET-mediated 5mC oxidation. *Cell* **2013**, *155*, 1545−1555.
(18) Lemke, E. A.; Summerer, D.; Geierstanger, B. H.; Brittain, S. M.; Schultz, P. G. Control of protein phosphorylation with a genetically encoded photocaged amino acid. *Nat. Chem. Biol.* **2007**, *3*, 769−772.
(19) Wang, J.; Liu, Y.; Liu, Y.; Zheng, S.; Wang, X.; Zhao, J.; Yang, F.; Zhang, G.; Wang, C.; Chen, P. R. Time-resolved protein activation by proximal decaging in living systems. *Nature* **2019**, *569*, 509−513.
(20) Ankenbruck, N.; Courtney, T.; Naro, Y.; Deiters, A. Optochemical Control of Biological Processes in Cells and Animals. *Angew. Chem., Int. Ed. Engl.* **2018**, *57*, 2768−2798.
(21) Courtney, T.; Deiters, A. Recent advances in the optical control of protein function through genetic code expansion. *Curr. Opin. Chem. Biol.* **2018**, *46*, 99−107.
(22) Baubec, T.; Ivanek, R.; Lienert, F.; Schubeler, D. Methylation-dependent and -independent genomic targeting principles of the MBD protein family. *Cell* **2013**, *153*, 480−492.
(23) Jorgensen, H. F.; Ben-Porath, I.; Bird, A. P. Mbd1 is recruited to both methylated and nonmethylated CpGs via distinct DNA binding domains. *Mol. Cell. Biol.* **2004**, *24*, 3387−3395.
(24) Fujita, N.; Takebayashi, S.; Okumura, K.; Kudo, S.; Chiba, T.; Saya, H.; Nakao, M. Methylation-mediated transcriptional silencing in euchromatin by methyl-CpG binding protein MBD1 isoforms. *Mol. Cell. Biol.* **1999**, *19*, 6415−6426.
(25) Clouaire, T.; de Las Heras, J. I.; Merusi, C.; Stancheva, I. Recruitment of MBD1 to target genes requires sequence-specific interaction of the MBD domain with methylated DNA. *Nucleic Acids Res.* **2010**, *38*, 4620−4634.
(26) Hameed, U. F.; Lim, J.; Zhang, Q.; Wasik, M. A.; Yang, D.; Swaminathan, K. Transcriptional repressor domain of MBD1 is intrinsically disordered and interacts with its binding partners in a selective manner. *Sci. Rep.* **2015**, *4*, 4896.
(27) Ichimura, T.; Watanabe, S.; Sakamoto, Y.; Aoto, T.; Fujita, N.; Nakao, M. Transcriptional repression and heterochromatin formation by MBD1 and MCAF/AM family proteins. *J. Biol. Chem.* **2005**, *280*, 13928−13935.
(28) Fujita, N.; Watanabe, S.; Ichimura, T.; Tsuruzoe, S.; Shinkai, Y.; Tachibana, M.; Chiba, T.; Nakao, M. Methyl-CpG binding domain 1 (MBD1) interacts with the Suv39h1-HP1 heterochromatic complex for DNA methylation-based transcriptional repression. *J. Biol. Chem.* **2003**, *278*, 24132−24138.
(29) Ng, H. H.; Jeppesen, P.; Bird, A. Active repression of methylated genes by the chromosomal protein MBD1. *Mol. Cell. Biol.* **2000**, *20*, 1394−1406.
(30) Schneider, C. A.; Rasband, W. S.; Eliceiri, K. W. NIH Image to ImageJ: 25 years of image analysis. *Nat. Methods* **2012**, *9*, 671−675.
(31) Ellis, B.; Haaland, P.; Hahne, F.; Le Meur, N.; Gopalakrishnan, N.; Spidlen, J.; Jiang, M.; Finak, G. *flowcore: Basic structures for flow cytometry data*; R package version 2.8.0.; 2022; DOI: 10.18129/B9.bioc.flowCore.
(32) Lo, K.; Hahne, F.; Brinkman, R. R.; Gottardo, R. flowClust: a Bioconductor package for automated gating of flow cytometry data. *BMC Bioinformatics* **2009**, *10*, 145.
(33) Lo, K.; Brinkman, R. R.; Gottardo, R. Automated gating of flow cytometry data via robust model-based clustering. *Cytometry A* **2008**, *73*, 321−332.
(34) Malek, M.; Taghiyar, M. J.; Chong, L.; Finak, G.; Gottardo, R.; Brinkman, R. R. flowDensity: reproducing manual gating of flow cytometry data by automated density-based cell population identification. *Bioinformatics* **2015**, *31*, 606−607.
(35) Hahne, F.; Gopalakrishnan, N.; Khodabakhshi, A. H.; Wong, C.-J.; Lee, K. *flowstats: statistical methods for the analysis of flow cytometry data*; R package version 4.8.0.; 2022; DOI: 10.18129/B9.bioc.flowStats.
(36) Van, P.; Jiang, W.; Gottardo, R.; Finak, G. ggCyto: next generation open-source visualization software for cytometry. *Bioinformatics* **2018**, *34*, 3951−3953.

https://doi.org/10.1021/acschembio.2c00245
ACS Chem. Biol. 2022, 17, 1844−1852